JTTEE5 10:67-75

Structure of Plasma-Sprayed Zirconia Coatings Tailored by Controlling the Temperature and Velocity of the Sprayed Particles

Marc Prystay, Patrick Gougeon, and Christian Moreau

(Submitted 15 January 1997; in revised form 7 June 2000)

The correlation between particle temperature and velocity with the structure of plasma-sprayed zirconia coatings is studied to determine which parameter most strongly influences the coating structure. The particle temperature and velocity are measured using an integrated optical monitoring system positioned normal to the spraying axis. The total porosity, angular crack distribution, and thermal diffusivity are correlated with the particle temperature and velocity. Results show that the temperature of the sprayed particles has a larger effect on the coating properties than the velocity in the conditions investigated.

Keywords angular crack distribution, image analysis, thermal barrier coatings, thermal diffusivity, particle diagnostics, zirconia

1. Introduction

In order to reliably engineer coatings with specific mechanical and physical properties, critical process control parameters must be identified. One approach to identify these parameters is to study how operating parameters affect coating properties.[1–4] A second approach is to develop on-line particle monitoring systems to measure the temperature and velocity of particles in flight.[5–11] Thus, rather than controlling the operating conditions of the torch, the properties of the sprayed particles are manipulated.

Much of this research is performed on stabilized zirconia coatings due to their wide application in the aerospace industry. The phase composition of zirconia coatings is affected by the spraying conditions, and the phase structure influences the thermal properties and stresses in the coating.[12–14] Moreover, the presence of cracks in sprayed coatings was shown to have a significant influence on the residual stress distribution.[15,16] In turn, cracks have been studied as a function of coating temperature,[17] and the effect of cracks on thermal diffusivity has been investigated.[18]

The goal of this paper is twofold. First, the influence of the torch operating parameters on the temperature and velocity of the sprayed particles is investigated. Second, the relation between particle velocity and temperature and the structure of plasma-sprayed zirconia coatings are studied. In particular, the angular crack distribution, porosity, and thermal diffusivity are examined in coatings prepared with particles sprayed at known temperature and velocity.

Marc Prystay, Patrick Gougeon, and **Christian Moreau,** National Research Council Canada, Industrial Materials Institute, Boucherville, PQ, Canada J4B 6Y4. Contact e-mail: christian.moreau@nrc.ca.

2. Particle Diagnostics and Spray Conditions

Particle temperature and velocity were monitored during plasma spraying using an integrated optical monitoring system, the DPV-2000, commercialized by Tecnar Automation Ltd. A detailed description of the monitoring system has been given in previous papers.[5,6] This system detects thermal radiation emitted by the hot particles as they pass in the measurement volume of the sensor head located near the plasma gun. When a particle passes in this measurement volume, its image is formed on a two-slit mask fixed on the end of an optical fiber, which guides light to the detection box located away from the plasma booth. The particle velocity is measured from the time of flight of the particle image between the two slits, and the measurement accuracy is better than 2%. Particle temperature is obtained by two-color pyrometry. The precision of the absolute temperature measurement depends on the actual optical properties of the sprayed materials, which is estimated to be 100 to 200 K. Furthermore, the diagnostic system allows measurement on the spray jet in its globality by analyzing all the radiation of the jet, which is received by a charge-coupled device (CCD) camera. From the analysis of this radiation profile, the diagnostic system finds the position of the spray jet axis relative to the torch.

In this work, particle diagnostics were achieved at 90 mm (3.5 in.) from the plasma torch during coating deposition at 100 mm from the torch. The coating temperature was controlled between 50 and 100 °C during deposition onto a copper substrate, which was sandblasted just before deposition. The plasma gun was of type SG-100 from Miller Thermal (Appleton, WI) and the spraying powder was yttria partially stabilized zirconia (Amdry 6643 fused and crushed, $-44 + 11$ μm). Particle diagnostics were performed in the center of the spray jet by using information from the CCD camera to achieve the measurement of velocity and temperature of particles having the same average trajectory. The data presented here are the numerical average values on the spray axis, and no attempts to analyze statistical distributions of parameters are presented. For each measurement, at least 900

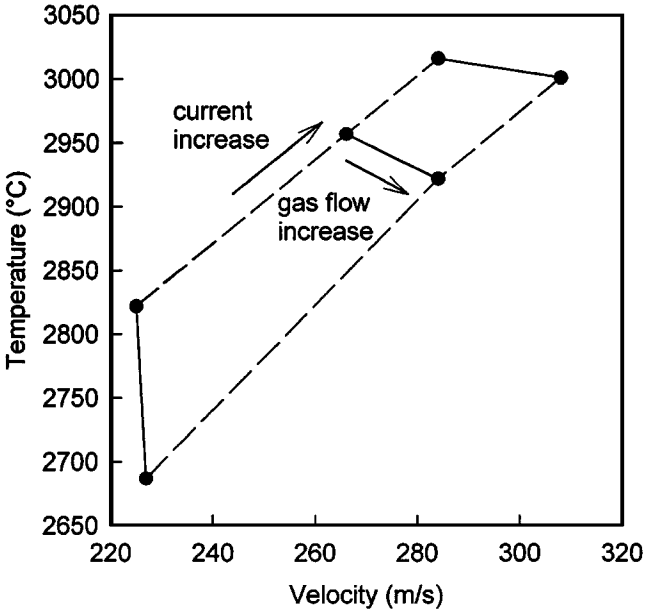

Fig. 1 Process control plot showing the effect of the arc current and arc gas flow rates on the particle temperature and velocity. The arc gas is Ar with 33% He and the powder is zirconia (−44 + 11 μm)

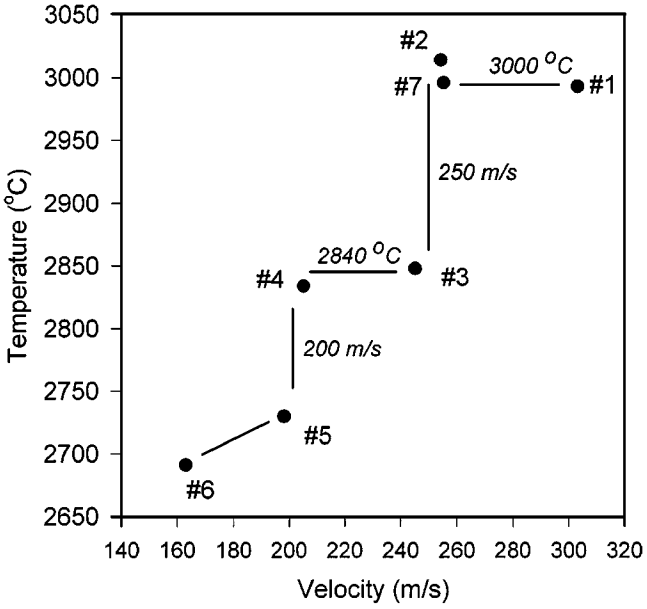

Fig. 2 Average temperature vs average velocity of the sprayed particles for each coating studied in this work. Numbers correspond to the specific coatings in Table 1

Table 1 Conditions of deposition and properties of zirconia samples

Coating number	1	2	3	4	5	6	7
Current (A)	900	925	600	500	525	500	925
Primary flow rate Ar (L/min)	61	42	56	42	56	50	42
Auxiliary flow rate He (L/min)	30	19	28	21	28	8	21
Powder feed rate (kg/h)	0.6	1.1	0.6	0.6	1.1	1.1	0.6
Average temperature (°C)	2990	3010	2850	2830	2730	2690	3000
Average velocity (m/s)	305	255	245	205	200	165	255
Deposition rate (μm/pass)	10	22	9	10	14	14	12
Porosity	15.3 ± 3.0	17.4 ± 1.8	18.6 ± 1.8	18.9 ± 2.7	17.6 ± 1.3	20.5 ± 2.5	15.7 ± 1.8
Thermal diffusivity ($\times 10^{-7}$ m^2/s)	5.0 ± 0.10	5.5 ± 0.05	4.8 ± 0.05	4.7 ± 0.10	4.5 ± 0.15	4.2 ± 0.05	5.0 ± 0.05

particles were analyzed, making the statistical error on the velocity measurement lower than 2 m/s and on the temperature measurement lower than 5 °C.

3. Coating Characterization

After the coatings cooled to room temperature, the copper substrates were etched away in 50% nitric acid heated to about 40 °C. Typically, 2 to 3 hours were required to remove all copper. No visible or microscopic differences could be detected between the samples before and after substrate removal. Coatings were measured to be 250 to 400 μm thick.

Thermal diffusivity measurements were made using the laser flash method. Samples were coated on the front and back surfaces with a thin (about 0.5 to 1.0 μm) coating of Au/Pd, which rendered the samples opaque to laser heating and to the detected wavelength. The calculation of thermal diffusivity followed the method of Degiovanni.[19,20] After thermal diffusivity measurements were completed, samples were infiltrated with epoxy, cut with a diamond saw, and polished following standard metallographic techniques. Samples were photographed under crossed polarized light at 500× magnification and the digital images stored to disk. Pullout caused by polishing was identified under polarized light as dark regions when the coating appeared transparent. These points were confirmed to be void of epoxy or ceramic under scanning electron microscopy and then removed from the photos before processing using digital image subtraction techniques.

Image analysis was performed on each photograph to measure the sample porosity and angular crack distribution. The algorithm developed treats each pore or crack as an individual feature of equal weighting. No results regarding the width are included. The algorithm applied is summarized in Appendix A. Results presented in this work are the accumulated sum of six images from a single cut. Repeated polishing and micrography produced the same results.

4. Results and Discussion

4.1 Selection of Spray Conditions

The thermal spray deposition conditions were chosen following a preliminary study that examined how the gases and

their mixture (pure argon, argon + helium, and argon + hydrogen) influenced the spray particles. For each of these conditions, the powder carrier gas flow rate was adjusted to position the spray jet axis at a constant angle of about 3° below the torch axis.

A process control plot showing the effect of the arc current and arc gas flow rate on the particle temperature and velocity is shown in Fig. 1. An increase in current increases both the temperature and velocity of the particles, whereas an increase in the gas flow rate increases the velocity but decreases the temperature. Subsequently, conditions for spraying particles at an exact temperature and velocity may be obtained by carefully regulating both the arc current and gas flow rates. From this study, it was decided to form coatings with Ar + He plasma gas and mainly with 33% He in the mixture.

A summary of the deposition conditions and coating characteristics is presented in Table 1. The measured temperature and velocity of the sprayed particles are plotted in Fig. 2. In general, the particle temperature and velocity are coupled; thus, as the particle velocity increases, so does the particle temperature. In addition, without changing the plasma torch configuration, it is difficult to obtain conditions of high velocity and low temperature or *vice versa*, which are represented in the top left and bottom right regions of the graph. Subsequently, it is not feasible to design simple studies that vary temperature or velocity over wide ranges independently in order to study their impact on the coating structure.

The velocity and temperature effects can be decoupled by selecting operating parameters to generate data points that fall along a staircase pattern. For example, the influence of particle velocity at about 3000 °C is seen by comparing coatings 1 and 7. (The average temperature between the particle temperatures of samples 1 and 7 is used. Other values shown on the graph were determined in the same manner.) The effect of velocity at particle temperatures of 2840 °C is seen by comparing samples 3 and 4. The results of changing particle temperature for fixed particle velocities are obtained by comparing sample 4 with 5 (200 m/s) and sample 3 with 7 (250 m/s). For completeness, it is noted in Table 1 that coating 6 was sprayed using an auxiliary gas content of 14% He, whereas all others were spray with a gas content of about 33% He. This was required to obtain the low temperature and velocity value with the SG100 plasma torch.

As indicated in Table 1, the powder feed rate was adjusted between 0.6 to 1.1 kg per hour in an attempt to have a similar coating thickness deposited per pass. Indeed, the deposition efficiency varies significantly according to the actual spray conditions. The obtained deposition rates were in the range of 9 to 14 μm per pass for all samples except for coating 2, where it reached 22 μm per pass. In fact, coating 2 was sprayed in the same particle conditions as coating 7 but with a higher powder feed rate, resulting in a deposition rate of 22 μm per pass as compared to 12 μm per pass for coating 2.

4.2 Coating Thermal Diffusivity and Porosity

The higher deposition rate of sample 2 has a significant influence on the coating diffusivity, as seen when comparing sample 2 with sample 7 in Table 1. It is now well established that the temperature of the surface on which the particles impinge has a dramatic influence on the flattening of the particles and on the quality of the contact between the lamellae within the coating.[18,21–26] The temperature of the surface on which the particles impinge depends on many parameters. With a high deposition rate per pass, the proportion of particles impinging on a hot surface is higher, as they impinge on the surface of lamellae deposited in the same pass and these lamellae are still at a relatively high temperature. In these conditions, it is expected that the mechanical contact between the lamellae deposited in one pass is better (lower interlamellar porosity), resulting, globally, in a lower thermal resistance between the lamellae and, consequently, in a higher thermal diffusivity of the coating.[18,21]

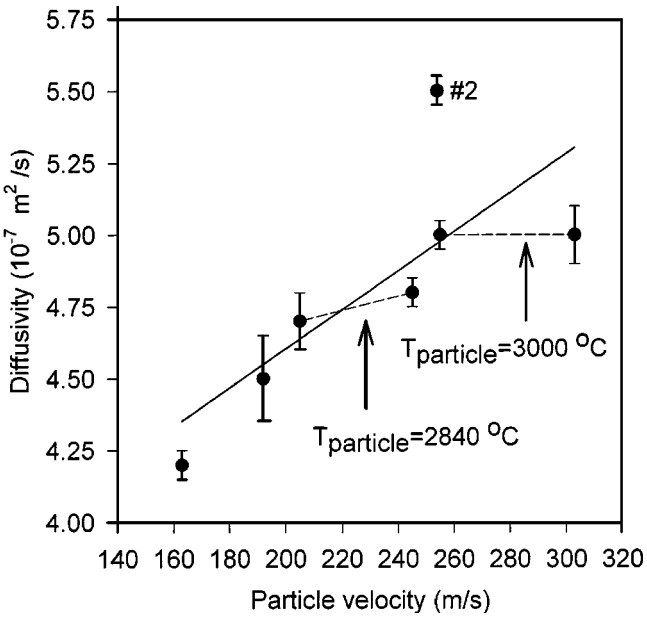

Fig. 3 Thermal diffusivity vs particle velocity. The solid line is the linear regression for all data points and the dashed line connects samples sprayed with the same particle temperature

Plots of thermal diffusivity versus the particle velocity and temperature are illustrated in Fig. 3 and 4, respectively. Sample 2 deposited using a higher deposition rate is indicated in the figure. The linear regression for all data (temperature and velocity coupled) is presented only to help visualize the trends. From these data, it can be seen that the thermal diffusivity generally increases with both the particle velocity and particle temperature. The points connected by the dotted lines represent the decoupled trends. When these data are examined, it is clear that the effect of velocity is minimal for a constant temperature (Fig. 3) and the effect of temperature is more pronounced at constant spraying velocities (Fig. 4). To relate this information to the coating structure, it is necessary to perform a metallographic examination of the coating cross section.

Trends in total porosity with particle velocity and temperature are presented in Fig. 5 and 6. The coupled data suggest that increased particle velocity and increased temperature create denser coatings, as indicated by the linear regression fit (solid line). The decoupled data (dashed lines) show that there may be a weak tendency toward denser coatings for higher particle velocities (Fig. 5), but porosity values for both temperature measurements fall within the same range when the error bars are

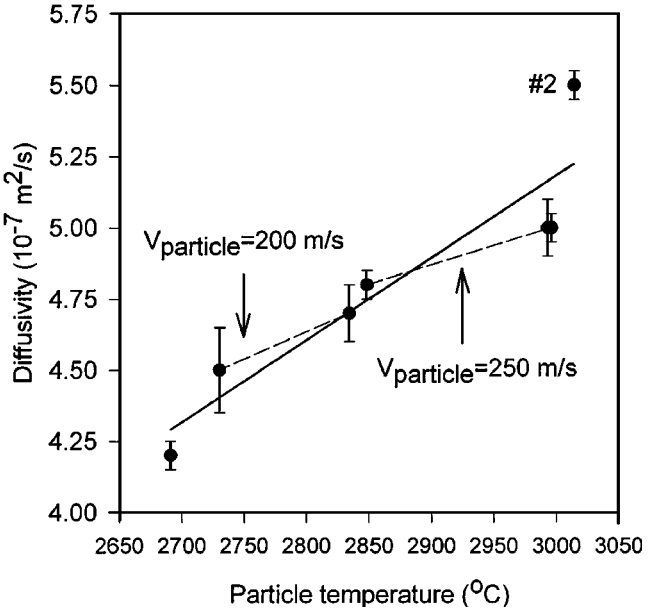

Fig. 4 Thermal diffusivity vs particle temperature. The solid line is the linear regression for all data points and the dashed line connects samples sprayed with the same particle velocity

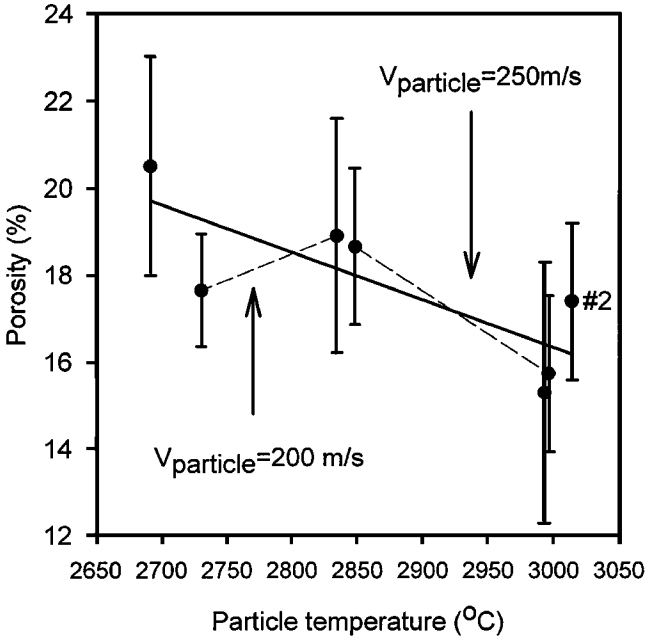

Fig. 6 Coating porosity vs particle temperature. The solid line is the linear regression for all data points and the dashed line connects samples sprayed with the same particle temperature

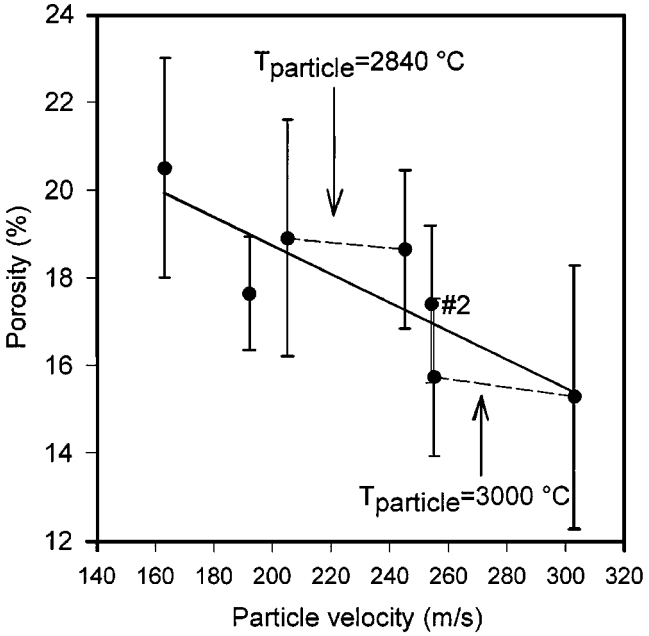

Fig. 5 Coating porosity vs average particle velocity. The solid line is the linear regression for all data points and the dashed line connects samples sprayed with the same particle temperature

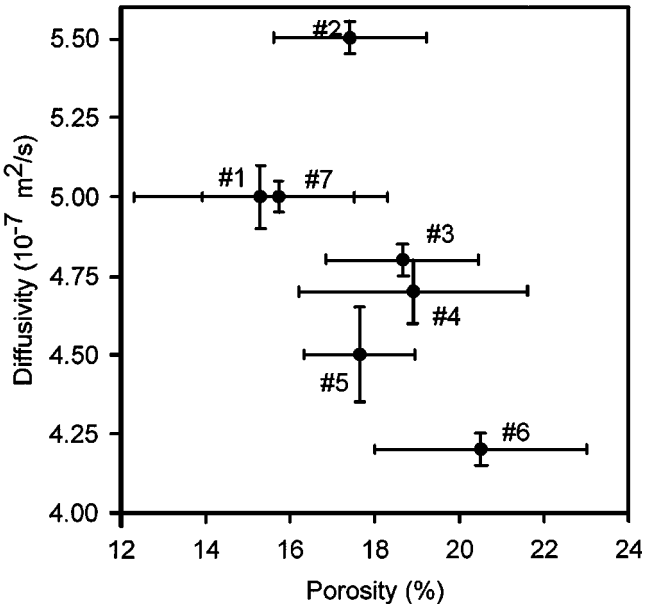

Fig. 7 Coating porosity vs thermal diffusivity. Each number corresponds to the samples in Table 1 and Fig. 2

considered. Similarly, the decoupled data for constant velocities of 200 and 250 m/s show relatively constant porosity for higher particle temperatures (Fig. 6). The inconclusive nature of the porosity correlation might be due to the small variations in the total porosity between coatings (15 to 19% porosity in the coatings with decoupled temperature and velocity) and the error bars due to variations seen locally under the microscope at 500× magnification. To study the influence on porosity more carefully, coatings with larger porosity variations need to be sprayed or results from significantly more micrographs need to be averaged.

A plot of thermal diffusivity versus porosity of plasma-sprayed zirconia coatings generally increases with decreasing coating porosity (Fig. 7). While the trend agrees with earlier

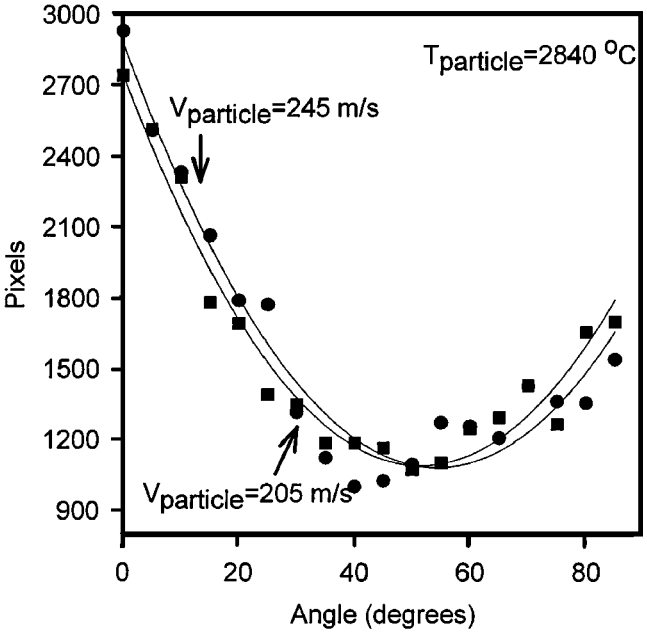

Fig. 8 Angular crack distribution in two coatings from particles sprayed at 2840 °C and (●) 245 m/s or (■)205 m/s. Cracks parallel to the surface are at 0°, while cracks perpendicular to the surface are at 90° in the plot

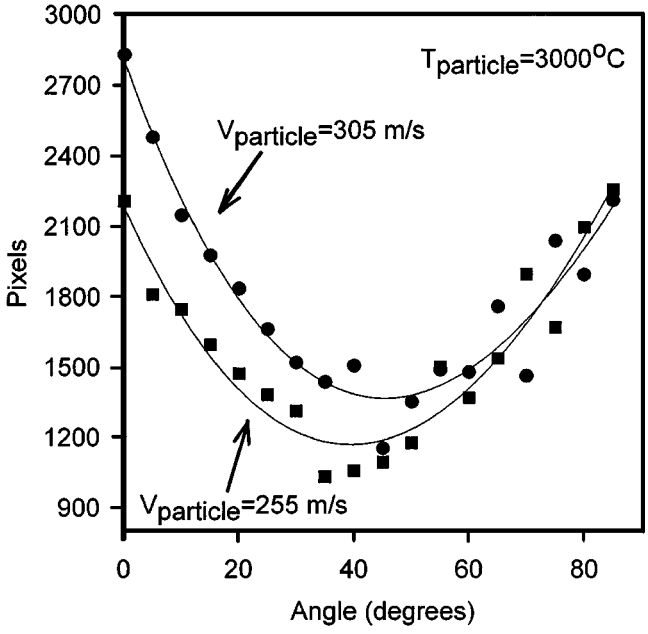

Fig. 9 Angular crack distribution in two coatings from particles sprayed at 3000 °C and (●) 305 m/s or (■) 255 m/s. Cracks parallel to the surface are at 0°, while cracks perpendicular to the surface are at 90° in the plot

findings,[27] no clear correlation between the two values was measured in our data. For example, if the diffusivity value of coating 2 (5.5×10^{-7} m^2/s) is ignored, the other six points form a strong tendency between diffusivity and porosity. However, if the diffusivity value of coating 6 (4.2×10^{-7} m^2/s) is ignored, there appears to be no correlation between diffusivity and porosity. It is noted that coating 6 was sprayed with an arc gas composition of 14% He, whereas all other coatings were sprayed with a composition of approximately 33% He.

It is not clear if the change in diffusivity is a coincidence or if the change in arc gas content affects the coating. Furthermore, no clear tendencies were seen in the decoupled data. This suggests that the diffusivity of the sample is not regulated by the total porosity alone. Rather, other factors such as the shape of the porosity and the relative phase content in the coating must also be considered.

4.3 Crack Distribution and Microstructure

The angular crack distributions for different particle conditions provide insight into how porosity can be controlled. The coating crack distributions from different particle velocities at temperatures of 2840 °C and 3000 °C are plotted in Fig. 8 and 9, respectively. The axis parallel to the substrate is considered as 0° and vertical cracks that propagate perpendicular to the substrate are at 90° on the plots. It is once again noted that the pixel counts represent the total length of the cracks and contain no information about the crack widths or location. With the magnification used in this study, the pixel width corresponds to a distance of about 0.4 μm in the coating cross-sectional plan.

At particle temperatures near 2840 °C, there is no significant difference in the coating structure between particles sprayed at 245 and 205 m/s (Fig. 8). Both coatings contain primarily horizontal cracks and there are relatively few vertical cracks. The differences in the curves are within experimental error. Particles sprayed at a higher temperature, 3000 °C, exhibit a difference in the horizontal crack distribution with spray velocity (Fig. 9). Coatings sprayed with particles at 255 m/s have similar horizontal and vertical structures, while coatings sprayed with particles at 305 m/s have increased numbers or longer horizontal cracks. The effect of higher spray velocities may be a physical lengthening of the horizontal cracks or the particles forming thinner splats. For the latter, the horizontal crack increase would be due to an increase in the number of cracks rather than the crack length. However, in either case, results suggest that the largest influence of the spray velocity is on horizontal cracks rather than on vertical cracks.

The angular distributions of cracks as a function of particle temperature are plotted for two spraying velocities in Fig. 10 and 11. At velocities of 200 m/s (Fig. 10), the effect of increased temperature is increased cracking in both the horizontal and vertical planes. At particle velocities of 250 m/s (Fig. 11), the increase in temperature has the effect of sharply decreasing the number of horizontal cracks and increasing the vertical cracking. In fact, particles sprayed at 250 m/s and 3000 °C exhibit only a weak preferred angular crack orientation. As mentioned previously, the quality of the mechanical contact between the lamellae influences the thermal diffusivity of the sprayed coatings. Indeed, extremely thin pores or cracks having a thickness of a few tenths of a micron are located at the interface between the lamellae.[14,22] In the present study, these fine horizontal cracks

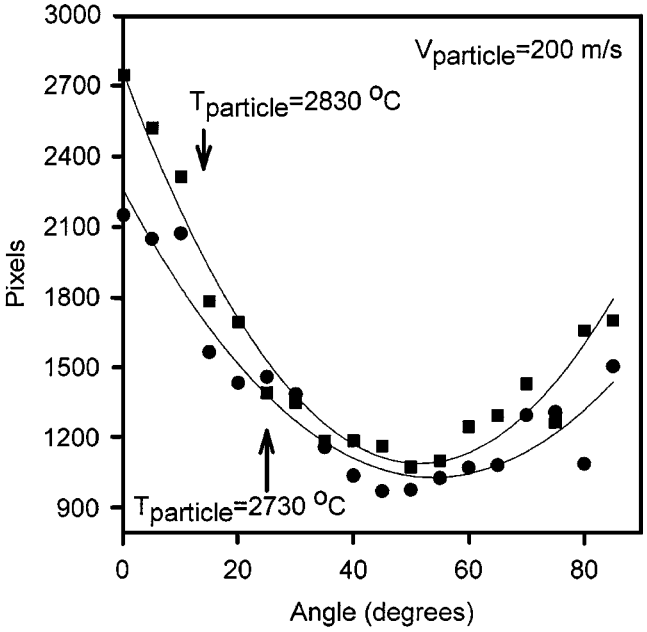

Fig. 10 Angular crack distribution in two coatings from particles sprayed at 200 m/s and (●) 2730 °C or (■) 2830 °C

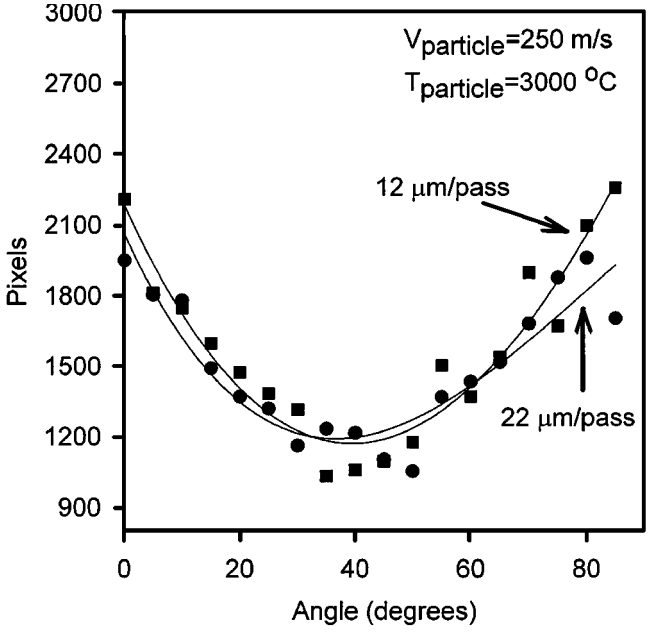

Fig. 12 Angular crack distribution in two coatings from particles sprayed at 250 m/s and 3000 °C with deposition rates of (●) 22 μm/pass or (■) 12 μm/pass

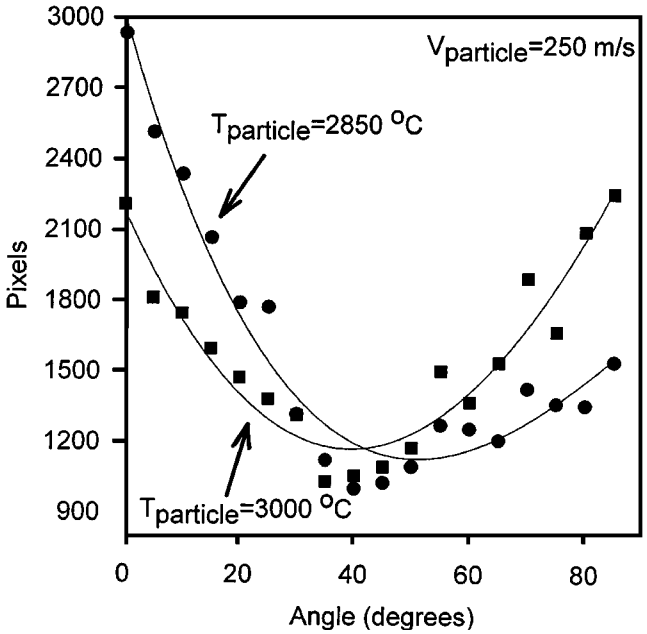

Fig. 11 Angular crack distribution in two coatings from particles sprayed at 250 m/s and (■) 3000 °C or (●) 2850 °C

are not taken into account, as they are too small to be observed under optical microscope while they can be detected by small-angle neutron scattering.[28] This is likely one of reason why there is no direct correlation observed between the total length of the horizontal cracks (Fig. 8 to 12) and the thermal diffusivity (Table 1).

Figure 12 shows that there is no significant difference between the crack distributions of the two coatings deposited with the same particle conditions but different deposition rates per pass (coatings 2 and 7). As mentioned previously, the higher thermal diffusivity of coating 2 is likely attributed to a better average thermal contact between the lamellae resulting from the higher deposition rate.

Images of coating 2 (255 m/s and 3010 °C) and coating 3 (245 m/s and 2850 °C) are presented in Fig. 13 and 14, respectively. Visually, it appears that coating 2 contains less orientation of the cracks than coating 3, which has cracks oriented primarily in the horizontal plane. Quantification of the differences in microstructure is difficult without a suitable image processing algorithm such as the one presented in Appendix A.

5. Future Work

The goal of this analysis was to study the influence of temperature and velocity of sprayed particles on coatings. It is understood that not all of the parameters that govern the coating structure have been taken into account. In particular, the stress in the coating may have been altered by removing it from the substrate, thereby relaxing the coating structure and changing the effect of the crack network on thermal diffusivity. Second, the phase distribution of the zirconia and the interlamellar porosity were not characterized and correlated to parameters such as thermal diffusivity. Nevertheless, the work presented here shows that the structure and angular crack network of the coating may be engineered by control of the temperature and velocity of the sprayed particles. This allows some control over the structure and thermal insulating properties of the coating.

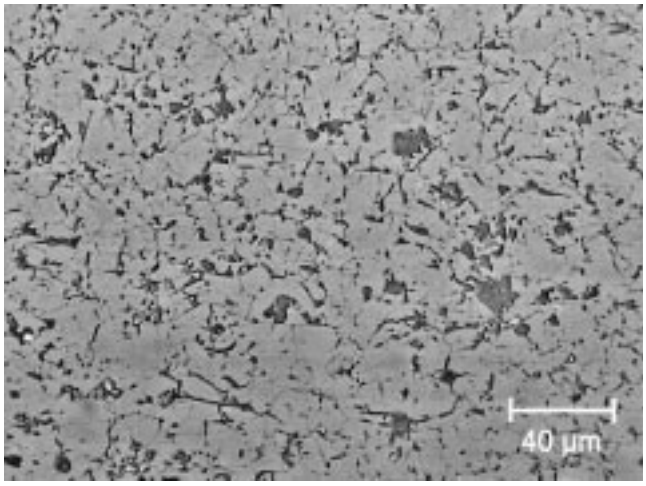

Fig. 13 Optical micrograph of coating 2 (255 m/s and 3010 °C) at 500× magnification

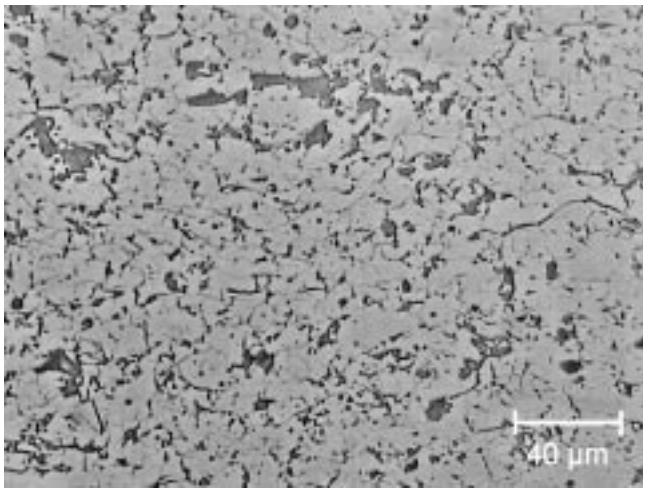

Fig. 14 Optical micrograph of coating 3 (245 m/s and 2850 °C) at 500× magnification. The microstructure contains more horizontal cracking that coating 2 shown in Fig. 12

It is clear that work in this field is important in identifying key process control parameters for the thermal spray industry. However, there remains significant effort ahead. For example, the powder size, substrate temperature, stand-off distance, and part geometry also directly affect the crack distribution and phase content of the coatings. This information will have to be collected and correlated to burner rig tests to determine optimal spraying parameters.

6. Conclusions

Particle temperature and velocity are key operating parameters that can be monitored in real time using an integrated optical approach. The conditions for spraying particles at a specific temperature and velocity may be obtained by carefully regulating both the arc current and gas flow rates. To study the effects of temperature and velocity, the two parameters should be decoupled by selecting conditions that generate a "staircase" plot, where one parameter is held constant while the other is varied (as in Fig. 2).

Metallographic analysis suggests that the particle temperature has a greater effect on the crack network and thermal diffusivity than does the velocity for the conditions used in this study. In general, higher velocities increased horizontal cracking, had no effect on vertical cracking, and had little or no effect on the coating diffusivity. On the other hand, higher particle spraying temperatures increase vertical cracking, might decrease horizontal cracking, and increase coating diffusivity. No clear correlation was found between thermal diffusivity and total porosity, suggesting other factors such as the shape of the porosity and the relative phase content in the coating must also be considered important.

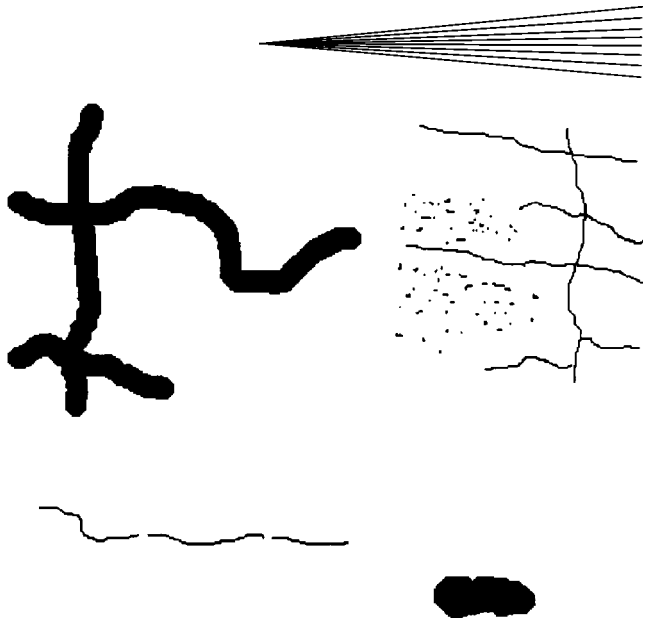

Fig. A1 A pictorial representation of a binary image. Details provided in text

Appendix A: Image Processing Algorithm

Samples were photographed under crossed-polarized light and the digital images stored to disk. Pullout caused by polishing was identified under polarized light as dark regions when the polarizers were adjusted so that the coating appeared transparent. Either photographs were taken in areas without pullout or pullout was removed from the image using digital image subtraction techniques.

Careful attention was accorded to uniform lighting. Corrections for minor nonuniformities in lighting were made with a high pass filter. A threshold was applied to the image and the binary representations were saved to disk. Due to the high contrast obtained under polarized light, only the finest cracks are difficult to threshold accurately. In such instances, the thresholding may result in some minor noise on the image. The most significant effect is a slight overestimation of the porosity in the coating. We

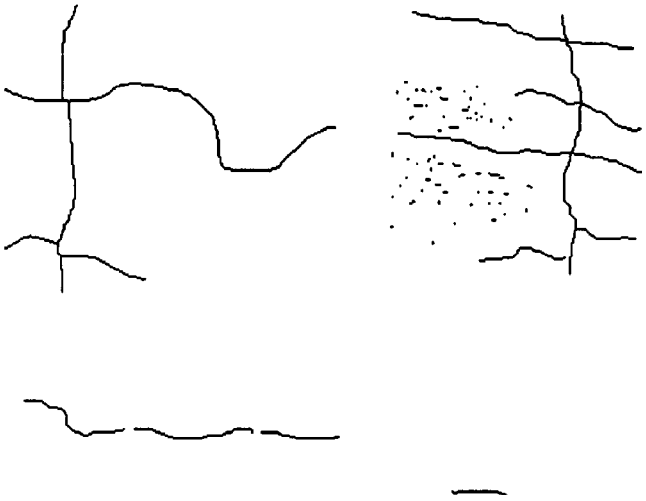

Fig. A2 Skeletonization of the image results in all cracks and pores being weighted by their length not their width

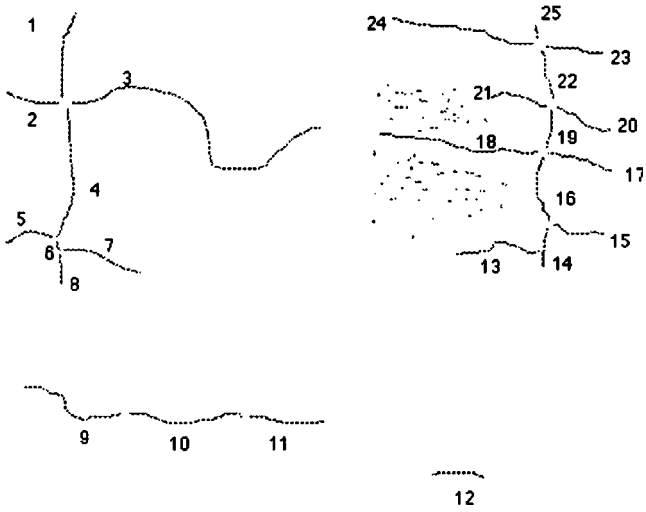

Fig. A3 The algorithm breaks all intersecting cracks into small cracks each having their own direction. In order to filter out noise in the image, only features with crack lengths greater than seven pixels are identified and analyzed

estimate a maximum absolute error of approximately 1 to 2%. However, as all images were processed following the same criteria, the relative error should be less.

A pictorial representation of a binary image is presented in Fig. A1. A large wide crack is depicted in the top left corner, a horizontal crack perceived to be chopped due to the propagation outside of the plane of polishing is in the bottom left corner, a pore is shown in the bottom right corner, and a fine crack network is shown in the top right corner. The dots and small cracks represent noise in the image that may accompany thresholding the fine crack network.

Using the binary image, pores and cracks are skeletonized so that they are one pixel wide (Fig. A2). As a result, pores and fine cracks are all weighted according to their length. Round pores with no directionality are reduced to a single pixel. Next, all intersecting cracks are identified and broken at the intersection. This gives the net effect of having several single cracks moving in specific directions rather than one large crack network (Fig. A3). Individual cracks are then identified, and their length, major axis, minor axis, and angle of propagation are recorded. By limiting the analysis to cracks over, say, seven pixels, the background noise in the image is filtered out. This filtering of small features is not found to distort the results, as the noise has little or no directionality.

For the purpose of this work, the cracks were binned from 0° (parallel to the substrate surface) to 90° (perpendicular to the substrate surface) in 5° steps. The graphs presented here are the accumulated sum of six independent images. Further information about the crack shapes is available by comparing the crack length to the major axis or plotting the histogram of the crack major axis divided by the minor axis length. We use similar analysis techniques to analyze pore size and shape distributions.

References

1. D. Bernard, M. Vardelle, A. Vardelle, and P. Fauchais: *Coll. Phys.*, 1990, Coll. C5 (Supp. 18), Tome 51, pp. 331-41 (in French).
2. T.C. Nerz, J.E. Nerz, B. A. Kushner, A.J. Rotolico, and W.L. Riggs: in *Thermal Spray: International Advances in Coatings Technology*, C. C. Berndt, ed., ASM International, Materials Park, OH, 1992, pp. 405-14.
3. T. J. Steeper, D.J. Varacalle, G.C. Wilson, W.L. Riggs, A.J. Rotolico, and J.E. Nerz: in *Thermal Spray: International Advances in Coatings Technology*, C. C. Berndt, ed., ASM International, Materials Park, OH, 1992, pp. 415-20.
4. M. Dorfman and J. DeBarro: in *Thermal Spray: International Advances in Coatings Technology*, C. C. Berndt, ed., ASM International, Materials Park, OH, 1992, pp. 439-46.
5. C. Moreau, P. Gougeon, M. Lamontagne, V. Lacasse, G. Vaudreuil, and P. Cielo: in *Thermal Spray Industrial Applications*, C. C. Berndt and S. Sampath, eds., ASM International, Materials Park, OH, 1994, pp. 431-37.
6. P. Gougeon, C. Moreau, V. Lacasse, M. Lamontagne, I. Powell, and A. Bewsher: *Adv. Processing Techniques Particulate Mater.*, 1994, vol. 6, pp. 199-209.
7. W.D. Swank, J.R. Fincke, and D.C. Haggard: in *Thermal Spray Science and Technology*, C.C. Berndt and S. Sampath, eds., ASM International, Materials Park, OH, 1995, pp. 111-16.
8. R.A. Neiser and T.J. Roemer: in *Thermal Spray: Practical Solutions for Engineering Problems*, C.C. Berndt, ed., ASM International, Materials Park, OH, 1996, pp. 285-93.
9. R.N. Wright, J.R. Fincke, W.D. Swank, and D.C. Haggard: in *Thermal Spray: Practical Solutions for Engineering Problems*, C.C. Berndt, ed., ASM International, Materials Park, OH, 1996, pp. 511-16.
10. A.C. Leger, M. Vardelle, A. Vardelle, P. Fauchais, S. Sampath, C.C. Berndt, and H. Herman: in *Thermal Spray: Practical Solutions for Engineering Problems*, C.C. Berndt, ed., ASM International, Materials Park, OH, 1996, pp. 623-28.
11. S. Sampath, J. Matejicek, C.C. Berndt, H. Herman, A.C. Leger, M. Vardelle, A. Vardelle, and P. Fauchais: in *Thermal Spray: Practical Solutions for Engineering Problems*, C.C. Berndt, ed., ASM International, Materials Park, OH, 1996, pp. 629-36.
12. R. Taylor, J.R. Brandon, and Paul Morrell: *Surface Coating Technol.*, 1992, No. 50, pp. 141-49.
13. T.A. Taylor: *Surface Coating Technol.*, 1992, No. 54-55, pp. 53-57
14. R. McPherson: *Surface Coating Technol.*, 1989, No. 39-40, pp. 173-81.
15 H.-J. Gross, W. Mallener, D. Strover, and R. Vassen: in *Thermal Spray Coatings: Research, Design and Applications*, C.C. Berndt and T.F. Ber-

necki, eds., ASM International, Materials Park, OH, 1993, pp. 581-85.
16. D.J. Greving, E.F. Rybicki, and J.R. Shadley: in *Thermal Spray Industrial Applications*, C.C. Berndt and S. Sampath, eds., ASM International, Materials Park, OH, 1994, pp. 647-53.
17. P. Bengtsson, T. Johanneson, and J. Wigren: in *Thermal Spraying: Current Status and Future Trends*, A. Ohmori, ed., High Temperature Society of Japan, Osaka, 1995, pp. 513-18.
18. S. Boire-Lavigne, C. Moreau, and R.G. Saint-Jacques: *J. Thermal Spray Technol.*, 1995, vol. 4, pp. 261-67.
19. A. Degiovanni: *Rev. Gen. Thermal Fr.*, 1977, pp. 185-417 (in French).
20. A.-S. Houlbert, P. Cielo, C. Moreau, and M. Lamontagne: *Int. J. Thermophys.*, 1994, vol. 15 (3), pp. 525-46.
21. R. McPherson: *Thin Solid Films*, 1994, vol. 112, pp. 89-95.
22. R. McPherson and B. V. Shafer: *Thin Solid Films*, 1982, vol. 97, pp. 201-04.
23. Y. Tanaka and M. Fukomoto: *Surface Coating Technol.*, 1999, vol. 120-121, pp.124-30.
24. M. Fukomoto, Y. Huang, and M. Ohwatary: in *Thermal Spray: Meeting the Challenges of the 21st Century*, C. Coddet, ed., ASM International, Materials Park, OH, 1998, pp. 401-06.
25. P. Fauchais, A. Vardelle, and M. Vardelle: *85th Meeting of the AGARD Structures and Materials Panel*, Advisory Group for Aerospace Research and Development (AGARD), Aalborg, Denmark, Oct. 1997, pp. 3-1 to 3-12.
26. S. Sampath, X.Y. Jiang, J. Matejicek, A.C. Leger, and A. Vardelle: *Mater. Sci. Eng.*, 1999, vol. A272, pp. 181-88.
27. L. Pawlowski, D. Lombard, and P. Fauchais: *J. Vac. Sci. Technol. A*, 1985, vol. 3 (6), pp. 2494-2500.
28. J. Ilavsky, G.G. Long, A.J. Allen, L. Leblanc, M. Prystay, and C. Moreau: *J. Thermal Spray Technol.*, 1999, vol. 8, pp. 414-20.